# Assessment of Constant-Potential Implicit Solvation Calculations of Electrochemical Energy Barriers for $H_2$ Evolution on Pt

Maxime Van den Bossche,[†,‡] Egill Skúlason,[‡] Christoph Rose-Petruck,[†] and Hannes Jónsson[*,‡]

†*Department of Chemistry, Brown University, Providence, RI, United States*
‡*Science Institute and Faculty of Physical Sciences, University of Iceland, 107 Reykjavík, Iceland*

E-mail: hj@hi.is

## Abstract

Theoretical estimation of the activation energy of electrochemical reactions is of critical importance but remains challenging. In this work, we address the usage of an implicit solvation model for describing hydrogen evolution reaction steps on Pt(111) and Pt(110), and compare with the 'extrapolation' approach as well as single-crystal measurements. We find that both methods yield qualitatively similar results, which are in fair agreement with the experimental data. Care should be taken, however, in addressing spurious electrostatic interactions between periodically repeated slabs in the VASPsol implementation. Considering the lower computational cost and higher flexibility of the implicit solvation approach, we expect this method to become a valuable tool in electrocatalysis.

## Introduction

Electrocatalytic reactions involve electron transfer to or from an electrode surface and are evidently crucial for all electrochemical production processes, as well as for corrosion chemistry and the electronics industry. Detailed insights into the reaction mechanism and kinetics, however, are difficult to obtain and generally require a combination of experimental and computational work.

While in classical, "gas phase" heterogeneous catalysis the field of theoretical modeling is rather well established, further methodological development is still required when it comes to electrocatalysis. Two major challenges in this field are given by (i) the description of metal/electrolyte interface, and (ii) the requirement of constant electrode potential over the course of an electron transfer reaction. These aspects complicate, in particular, the evaluation of activation energies of electron transfer reactions. As a result, the vast majority of computational electrocatalysis studies have been limited to thermodynamic properties only, such as reaction energies.[1,2] It is, however, well recognized that the proper study of reaction kinetics (in electrocatalysis as in conventional catalysis) requires knowledge of transition state energies.[3,4]

Several approaches have so far been proposed to address these challenges, which differ especially in the manner the constant-potential requirement is handled. This requirement stipulates that the electrode potential w.r.t. the reference electrode remains constant over the course of an elementary reaction, also when it is accompanied by electron transfer. As only a finite number of electrons $N_e$ can be included in the electronic structure calculations, however,

the potential will change significantly over the course of an electron transfer reaction, if $N_e$ is held constant.[5–7] Extended electrode surfaces are furthermore most conveniently modeled using periodically repeated supercells, which must satisfy overall charge neutrality.

In this context, the arguably most rigorous method is the so-called 'extrapolation' approach,[5,6] where energy barriers are evaluated at successively larger lateral cell dimensions and extrapolated to the infinite cell limit where the potential drop is zero. The number of electrons $N_e$ is determined by the charge neutrality condition, which entails that e.g. hydrogen atoms must be added to or withdrawn from the electrolyte to vary the electrode potential. This method has so far exclusively been applied to FCC(111) surfaces in conjunction with ice-like hexagonal water structures.[5,6,8,9]

In a second, related method,[10,11] the computationally costly extrapolation is avoided by assuming that the required correction to the transition state energy has a purely capacitive character. This correction is based on changes in the charges of the metal atoms at the electrode surface, and hence an additional ambiguity lies in the choice of the charge density partitioning scheme.

Thirdly, in the 'double reference' approach[12,13] the electrode potential is controlled by varying $N_e$, with introduction of a homogeneous compensating background to maintain overall charge neutrality. It is not quite clear, at this point, if this method applies sound corrections to the obtained total energies, which is known to be a non-trivial problem in the case of charged slabs in homogeneous compensating backgrounds.[14,15]

Methods have also been proposed where charge neutrality is maintained by localizing the compensating charge in a 'counter-electrode' at some distance away from the electrode/electrolyte interface.[16,17] In reality, however, charge compensation is mediated by changes in the concentration profiles of the electrolyte's ions near the electrode surface.

In yet another approach[18,19] electrochemical barriers are estimated in a two-step procedure inspired by Markus theory. First, the activation energy of the corresponding non-electrochemical reaction is calculated (e.g. reaction with adsorbed H in the case of a proton-coupled electron transfer (PCET) reaction) and it is assumed that, at the same potential, the electrochemical process possesses the same activation energy. The potential dependence of the activation energy is then described using e.g. Butler-Volmer theory, requiring further simplifying assumptions regarding the symmetry factor of the reaction.

Finally, a more recently developed approach, which we will be focusing on in this work, is one where (part of) the electrolyte is approximated by a polarizable dielectric continuum (i.e. an implicit solvation model).[20–23] The constant-potential requirement is here obeyed by varying $N_e$ with concomitant changes in the concentration of counterions in the surrounding electrolytes (frequently described by Poisson-Boltzmann theory). The main assumption here, then, is that the ionic distribution in the electrolyte is equilibrated also at the saddle point, and not only at the reactant and product states.

Although several studies have applied the above constant-potential approach with implicit solvation models (using e.g. the VASPsol,[24–27] JDFTx,[28] SIESTA[29–33] and GPAW codes[34]), we are not aware of attempts to compare its results to those of the extrapolation method, or to detailed single-crystal measurements.

The present work offers such a comparison, focusing on the various steps of the hydrogen evolution reaction (HER) on Pt(111) and Pt(110). There are three types of reactions relevant to the HER:

$$\text{Volmer:} \quad \mathrm{H^+ + e^- + {}^* \rightarrow H^*} \tag{1}$$

$$\text{Tafel:} \quad \mathrm{2\,H^* \rightarrow H_2 + 2\,{}^*} \tag{2}$$

$$\text{Heyrovský:} \quad \mathrm{H^+ + e^- + H^* \rightarrow H_2 + {}^*} \tag{3}$$

Adsorbed H and vacant adsorption sites are denoted $H^*$ and $^*$, respectively.

The (111) facet is chosen to compare with the extrapolation approach, which has so far been exclusively applied to FCC(111) surfaces due to the commensurability with the hexagonal ice bi-

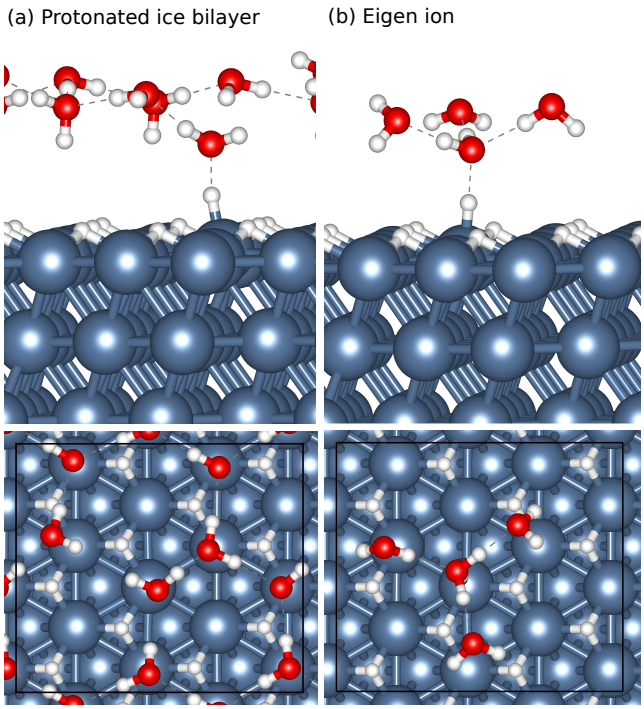


Figure 1: Side and top views of the obtained transition states at 0 $V_{SHE}$ for the Volmer reaction on Pt(111) at an initial hydrogen coverage of 0.92 ML. The considered water structure are a protonated hexagonal ice bilayer [Panel (a)] and a $H_3O^+(H_2O)_3$ ('Eigen') cation [Panel (b)].

layer structure used to model the metal/water interface. The structure of this adlayer is illustrated in Figure 1, in the transition state for hydrogen deposition via the Volmer reaction. As the implicit solvation approach is less restricted in terms of water structures, we will also compare with results from a water cluster model, corresponding to the 'Eigen' cation in its protonated form ($H_3O^+(H_2O)_3$). As the equilibrium H coverage on Pt(111) at 0 $V_{SHE}$ has been calculated to be circa 0.9 ML using the RPBE functional,[6] we will focus on HER reactions involving H atoms adsorbed in threefold hollow sites at a coverage of up to 1 ML. Also, the HER steps on (110) facets are included, as experimental Tafel slopes are here easier to analyze and indicate a Volmer-Tafel mechanism with the Tafel reaction as the rate-determining step (RDS).[35]

It should be noted that the above considerations apply not only to activation energies but also to reaction energies. The latter have, however, typically been calculated using the computational hydrogen electrode (CHE) formalism,[1] which makes use of the equilibrium relation of the proton/hydrogen redox-couple of the standard hydrogen electrode (SHE). The focus of this work will hence lie on the estimation of barrier heights.

# Computational methods

To facilitate the comparison to results from previous publications with the extrapolation approach,[6] the same computational setup is used here. The bulk of the electronic structure calculations are performed with the VASP code[36–39] using Kohn-Sham density functional theory (DFT).[40,41] Core electrons are treated via standard projector augmented wave (PAW) setups with the following valences: H (1), O (6), Pt (10). The basis set consists of plane waves with a kinetic energy up to 350 eV.

Additional calculations are carried out using the JDFTx code[21] employing GBRV ultrasoft pseudopotentials[42] with the recommended cutoffs for the wave functions (20 Hartree) and the electron density (100 Hartree).[1]

Electronic exchange and correlation are described using the revised Perdew-Burke-Ernzerhof (RPBE) functional[43] which modifies the exchange enhancement factor of the original PBE expression[44] to improve the description of adsorption energies on transition metal surfaces. In JDFTx the RPBE functional is implemented through the LibXC library.[45]

Three-layer slabs of $c(3\times4)$ geometry are employed for the Pt(111) surface, with the RPBE crystal lattice constant of 4.025 Å. For the Pt(110) slab, six metal layers are used with a $p(2\times4)$ cell size and a $(1\times2)$ missing-row reconstruction. In both cases the first Brillouin zone is sampled using $(4\times3\times1)$ Monkhorst-Pack grids.[46,47] Local minimizations and saddle point searches with the dimer method [48,49] are pursued until the largest force components are less than 0.05 eV/Å in magnitude. All metal layers except the topmost layer are constrained to their bulk lattice positions. The distances

[1] In the GBRV pseudopotential set the $5p^6$ semicore states are included in the valence for Pt.

separating periodically repeated slabs will be addressed in the Results section.

Implicit solvation calculations of the aqueous electrolyte are performed using the GLSSA13 solvent model,[50] which is available in VASP through the VASPsol extension.[22,23] Like other models such as SCCS,[51] the method puts forward a dielectric profile $\epsilon$ as a functional of the Kohn-Sham electron density distribution $\rho$:

$$\epsilon[\rho] = 1 + (\epsilon_{\text{bulk}} - 1)\, S[\rho], \tag{4}$$

with the following form for the 'shape function' $S$:

$$S[\rho] = \frac{1}{2}\text{erfc}\left(\frac{\log\left(\rho/\rho_{\text{cut}}\right)}{\sigma\sqrt{2}}\right). \tag{5}$$

The dielectric function therefore changes gradually from 1 to the bulk dielectric constant $\epsilon_{\text{bulk}}$ (78.4, the experimental value for liquid water at 298 K[52]). The particular shape of this transition is governed by the $\sigma$ and $\rho_{\text{cut}}$ parameter, for which we have applied the default values (0.6 and 0.0025 Å$^{-3}$, respectively). The free energy required to create a solvent cavity around the solute is calculated as

$$\text{A}_{\text{cavity}} = \tau \int |\nabla S| d\mathbf{r}, \tag{6}$$

where the $\tau$ parameter (0.525 meV/Å$^2$) has been optimized to reproduce the solvation energies of a series of organic molecules.[22]

In case the electrode potential is different from the potential of zero charge (PZC), a counterion charge distribution is included in the implicit solvent region through the use of the generalized Poisson-Boltzmann equation:

$$\nabla \cdot \epsilon(\mathbf{r}) \nabla \phi_{tot}(\mathbf{r}) = \left(\frac{2c_0 q^2 e^2}{k_B T}\right) \phi_{tot}(\mathbf{r}) - \rho_{solute}(\mathbf{r}), \tag{7}$$

$$c_{\pm}(\mathbf{r}) = c_0 \exp\left(\frac{\pm q\, e\, \phi_{tot}(\mathbf{r})}{k_B T}\right) S\left[\rho(\mathbf{r})\right]. \tag{8}$$

We used $\kappa$ values corresponding to a Debye length of 3 Å, corresponding to a 1 M concentration of a 1:1 electrolyte ($c_0$ =1 M). This mimics the experimental situation where 1 M of a strong acid is used ($\text{U}_{\text{SHE}} = 0$ for HER and pH = 0).

Though grand-canonical SCF algorithms exist[21] which vary the number of electrons $N_e$ so as to match the targeted chemical potential, currently only conventional (canonical) methods are available in VASPsol, making it necessary to adjust $N_e$ in between successive SCF loops instead. For local minimization runs, we use a simple iterative approach:

$$N_e(i+1) = N_e(i) - a \cdot \left[\mu_e(i) - \mu_{e,\text{target}}\right]. \tag{9}$$

We find an $a$ value of 1.0 V$^{-1}$ to be appropriate for the structures considered in this work. In this manner, the electrode potential converges to the targeted value as the local optimization proceeds. For saddle point searches, we find it more convenient to adapt $N_e$ after a completed dimer search, iterating until the target potential is matched within 15 mV.

The electronic chemical potential $\mu_e$ is calculated by comparing the Fermi level with the potential in the bulk electrolyte, which in an implicit solvent equals that of an electron in vacuum:[23]

$$\mu_e = \epsilon_{\text{Fermi}} - V_{\text{bulk}}. \tag{10}$$

It should be noted that the use of Equation (10) is not restricted to symmetric slab structures, as the electrolyte screens the dipole moment of the solute, resulting in a zero net dipole moment and therefore also in a flat electrostatic potential in the bulk solvent region. If, then, a certain potential $U$ is to be attained w.r.t. the standard hydrogen electrode (SHE), the target chemical potential is given by:

$$\mu_{e,\text{target}} = -\Phi_{\text{SHE}} - U, \tag{11}$$

where $\Phi_{\text{SHE}}$ is the work function of the SHE. We have taken $\Phi_{\text{SHE}}$ equal to 4.43 V, which lies within the experimental value of the SHE work function compared to vacuum which is usually measured to be 4.44 (+/- 0.02) V.[53]

To compare energy differences of two structures at different $N_e$ values (but identical electrode potential $U$), the VASPsol and JDFTx output energies need to be corrected by the cost

(gain) of removing (adding) electrons:

$$\Omega = E_{\mathrm{DFT}} + N_{\mathrm{e}}\,\mu_{\mathrm{e}}(U). \tag{12}$$

Even though $E_{\mathrm{DFT}}$ here includes entropy terms from the solvation model, we will refer to $\Delta\Omega$ as (electronic) grand-canonical energy differences, as no entropic contributions are included in the DFT calculations.

The symmetry factor $\beta$ for an elementary reaction at a given $U$ corresponds to the derivative of the activation energy w.r.t. $U$, which we evaluate using a central difference scheme ($\Delta U = 0.1$V):

$$\beta(U) = \frac{\partial \Delta\Omega_{\mathrm{act}}}{e\,\partial U}, \tag{13}$$

$$\simeq \frac{\Delta\Omega_{\mathrm{act}}(U+\Delta U) + \Delta\Omega_{\mathrm{act}}(U-\Delta U)}{2e\Delta U}. \tag{14}$$

# Results and Discussion

In the following paragraphs we present our results for Volmer, Tafel, and Heyrovský energy barriers on Pt(111) and Pt(110) at $U = 0$ V on the SHE scale.

## $H_2$ evolution on Pt(111)

### Convergence w.r.t. slab separation

The activation energies calculated with VASPsol (following the procedure outlined in the previous Section) are found to converge only slowly with respect to the distance $L_z$ between periodically repeated slabs. More precisely, the activation energies are a linear function of $1/L_z$, as shown in Figure 2. The slopes of the fitted regression lines appear to be anti-correlated to the difference in $N_e$ between the initial and transition states. The slope is namely close to zero for the Tafel reactions (for which $\Delta N_e \simeq -0.05\,\mathrm{e}^-$) and negative for the Volmer and Heyrovský reactions (where $\Delta N_e \simeq 0.6\,\mathrm{e}^-$). Importantly, however, the calculated electrode potential is found to remain constant upon variation of $\mathrm{L}_z$, with deviations of at most 30 mV.

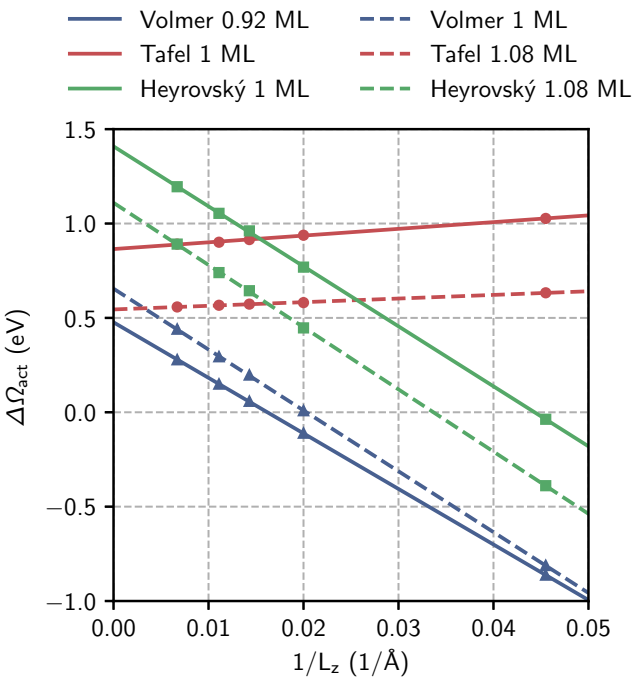


Figure 2: Activation energies calculated at 0 $\mathrm{V_{SHE}}$ using VASPsol for HER reactions on Pt(111) using Eigen ions as a proton model for the PCET reactions. The values are plotted as function of the inverse of the cell length perpendicular to the plane of the slab. The three types of barriers have been evaluated at two different hydrogen coverages in the reactant state, i.e. at/below 1 ML and above 1 ML.

The $1/L_z$ dependence suggests the presence of spurious charge interactions in the conventional 3D-periodic implementation in VASPsol. This behavior is possibly connected to the observation that standard Poisson-Boltzmann models do not necessarily enforce strict charge neutrality.[54] We therefore performed single-point calculations using the JDFTx code which implements a truncated Coulomb scheme to fully decouple periodically repeated slabs.[55] As shown in Table 1, the JDFTx activation energies indeed agree well with the VASPsol results extrapolated to $L_z = \infty$. The small differences that remain can be attributed to the different treatments of core-valence interactions and kinetic energy cutoffs.

It should furthermore be noted that the $L_z$-dependence seems not to have been taken into account in several previous studies[24,25,27]

**Table 1: Comparison of VASPsol activation energies (obtained at 0 $V_{SHE}$ and extrapolated to $L_z = \infty$)and JDFTx single-point calculations performed at the VASPsol geometries using a Coulomb truncation scheme. Each barrier has been evaluated at two different initial hydrogen coverages $\theta_H$ as well as two different water structures (a water cluster corresponding to the 'Eigen' cation as well as the (protonated) ice bilayer ('IBL') structure).**

| | | $\Delta\Omega_{act}$ (eV) | | | |
|---|---|---|---|---|---|
| Reaction | $\theta_H$ (ML) | VASPsol (Eigen) | JDFTx (Eigen) | VASPsol (IBL) | JDFTx (IBL) |
| Volmer | 0.92 | 0.477 | 0.479 | 0.692 | 0.693 |
| | 1.00 | 0.655 | 0.629 | 0.805 | 0.838 |
| Tafel | 1.00 | 0.865 | 1.007 | 0.807 | 0.830 |
| | 1.08 | 0.545 | 0.407 | 0.420 | 0.416 |
| Heyrovský | 1.00 | 1.408 | 1.364 | 1.618 | 1.625 |
| | 1.08 | 1.110 | 0.995 | 1.393 | 1.388 |

of PCET reactions using the VASPsol code. Without extrapolation to $L_z = \infty$, values of $L_z$ of over 400 Å would be have been required in the present work to converge the Volmer and Heyrovský barriers on Pt(111) within 0.1 eV. Moreover, without extrapolation one may even obtain negative activation energies if too low $L_z$ values are employed, as shown in Figure 2).

## Water model

Figure 3 furthermore shows the barrier heights when an ice bilayer is used for the water structure (red bars), compared to the results with an Eigen ion (blue bars).[2] The two sets are in fair agreement, though it can be noticed that the barriers for the PCET reactions (i.e. Volmer and Heyrovský steps) are consistently increased by about 0.2 eV when employing the ice bilayer model. We attribute this difference, in part, to the relative rigidity of the bilayer structure, leading to a more pronounced loss (compared to the more 'flexible' water cluster model) of hydrogen bonds in the transition state than in the initial state. The changes in H-bond distances are reported in Table 2 for the Volmer reaction (the corresponding transition state structures are shown in Figure 1). For the water cluster, the coordination of the central $H_3O^+$ ion is qualitatively similar in the initial and transition states: 2 H-bonds are donated, and 1 H-bond is accepted. Using the ice bilayer, however, the $H_3O^+$ ion at the saddle point is significantly less well solvated compared to the initial state: two fewer H-bonds are donated, and only one more (stretched) H-bond is accepted. Another difference between the two water models is that the next-nearest neighbor water molecules are described explicitly in the bilayer model, and are substituted by implicit solvent in the cluster model, which may also contribute to the difference in activation energies. Though the structural properties of the water/Pt(111) interface remains an active field of research [56,57], several theoretical and experimental works have provided support for ice bilayer formation on Pt(111).[58–61] An interesting yet unanswered question, in this regard, is how fast or slow the dielectric properties of the electrolyte approach that of the bulk in case an ice-like (bi)layer is formed at the surface. The choice of the bulk dielectric constant in the present implicit solvent calculations presumes that the convergence rate is similar to that at a liquid water/metal interface.

This suggests that the energy barrier obtained with the bilayer structure would be more accurate than with the cluster model. As will be discussed further below, however, the Volmer and Heyrovský steps are not kinetically relevant

[2]Note that the Tafel barriers reported in the 'water cluster' approach are calculated without explicit water molecules.

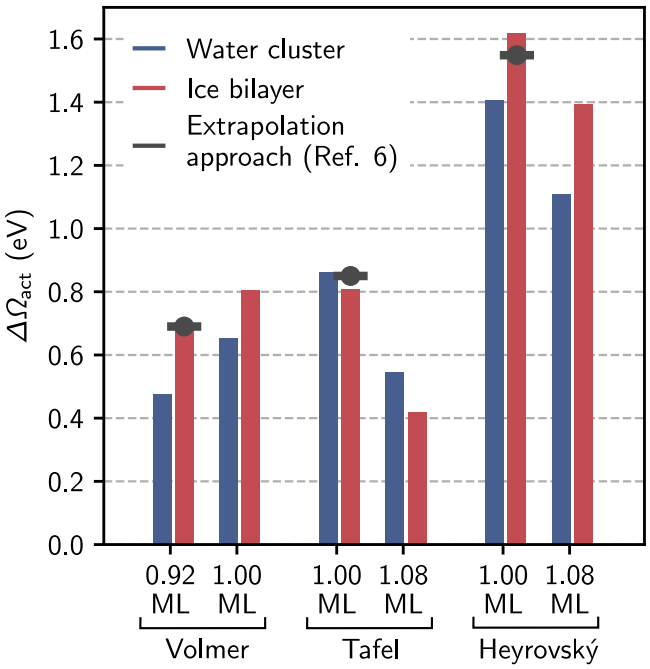


Figure 3: Activation energies for HER reactions on Pt(111) calculated at 0 $V_{SHE}$ using the implicit solvation scheme (VASPsol) at different initial hydrogen coverages and with two different water structures. The values obtained via the extrapolation approach are also indicated (see Ref. 6)

.

for HER on Pt(111) at 0 $V_{SHE}$, and therefore the relative accuracy of the two water models cannot be compared in this context.

**Table 2: Hydrogen-bond distances in Å for the $H_3O^+$ ion at the initial state (IS) and transition state (TS) for the Volmer step on Pt(111) with an initial H coverage of 0.92 ML at 0 $V_{SHE}$.**

| Water structure | Donor | Acceptor |
|---|---|---|
| Water cluster (IS) | 1.39, 1.39 | 2.09 |
| Water cluster (TS) | 1.75, 1.80 | 1.94 |
| Ice bilayer (IS) | 1.45, 1.59, 1.58 | - |
| Ice bilayer (TS) | 1.70 | 2.46 |

## Comparison with the extrapolation approach

The calculated barrier heights are now compared with literature results obtained with the extrapolation at the same electrode potential, hydrogen coverage, and water model (the ice bilayer structure, see Ref. 6) as also shown in Figure 3.[3] The agreement is remarkably good, considering the pronounced differences in methodology. Both approaches therefore agree that hydrogen is evolved via a Volmer-Tafel mechanism with the Tafel step as the RDS at 0 V w.r.t. SHE.

Additionally, Figure 3 shows that with the implicit solvation approach the barriers change as the coverage is increased beyond 1 ML, in ways which are similar to the extrapolation approach.[6] Increasing the coverage beyond 1 ML requires the occupation of the energetically less favorable atop sites. Following a Bell-Evans-Polanyi principle, the activation energy for the Volmer step increases, whereas those of the Tafel and Heyrovský steps decrease.

Lastly, the symmetry factors $\beta$ calculated at 0 $V_{SHE}$ with the ice bilayer model amount to 0.62 (Volmer, $\theta_H$ = 0.92 ML), -0.04 (Tafel, $\theta_H$ = 1 ML), and 0.76 (Heyrovský, $\theta_H$ = 1 ML). The symmetry factors are mainly determined by the amounts of charge transfer from the initial state to the saddle point, which are calculated to be 0.58, -0.07 and 0.62 electrons, respectively. The activation energies of the two PCET reactions will therefore indeed decrease as the applied potential is lowered, while the barrier for the non-electrochemical Tafel step is nearly potential-independent. Skúlason and coworkers[6] obtained values of 0.44, ∼0, and 1.07, respectively, using the extrapolation approach. These values are, however, not directly comparable to ours, as these also include the potential dependence of the hydrogen coverage and of the transition state geometry and are obtained by linear regression over a fairly wide potential range of 1 V or more.

[3] In Ref. 6 the Heyrovský barrier at an initial H coverage of 1 ML is given at -0.2 $V_{SHE}$. We therefore used a typical symmetry factor of 0.5 to estimate the corresponding value at 0 $V_{SHE}$.

### Comparison with experimental measurements

Experimental measurements of the HER kinetics on Pt(111) surfaces are available in the works by Marković et al.[35] and He et al.[62] Although both groups measure similar current densities at 0 V, different temperature dependencies are reported. We follow the explanation offered in Ref. 62 that the Pt(111) substrate used in Ref. 35 may have contained low concentrations of highly active defect sites. In this view, the higher apparent activation energy measured by He et al., 0.67 eV, should be closer to that of a pristine Pt(111) surface. The magnitude of the corresponding pre-exponential factor (circa $10^{10}$ mA/cm$^2$) is characteristic of a process involving only surface adsorbates, supporting the Tafel reaction as the RDS. These findings therefore qualitatively agree with the computational results described in the previous paragraphs, where the same Tafel RDS is found, though with a somewhat higher activation energy (0.80-0.85 eV). As the barrier for the Tafel step is not sensitive to the water structure at the interface, this does not, unfortunately, allow to discriminate between different types of water models.

### Comparison with other implicit solvent calculations

Fang et al. have previously addressed[31] the HER on Pt(111) using a similar method implemented in the SIESTA code.[32,33] At 0 $V_{SHE}$ and a hydrogen coverage at or below 1 ML, the Tafel barrier reported by Fang et al. (0.92 eV) agrees well with our calculations, while the reported Volmer and Heyrovský barrier heights are significantly lower than ours ($< 0.2$ eV and 0.93 eV, respectively). In attempting to locate the origins of this difference for the Volmer reaction, we find that the inclusion of zero-point vibrational energy corrections lowers the calculated barrier by 0.10 eV, while applying the PBE functional only decreases the barrier by 0.03 eV compared to RPBE. The use of a water trimer cluster with the PBE functional, however, increases the barrier by 0.16 eV compared to the tetramer. This suggests that the influence of e.g. the different basis set types and implicit solvent models needs to be investigated to elucidate the remaining discrepancies.

An alternative constant-potential implicit solvation approach has been recently proposed[34] where essentially the countercharge is not described by a Poisson-Boltzmann equation, but is instead homogeneously spread out over a part of the bulk solvent region. Using this 'solvated jellium method' (SJM), the barrier for the Volmer step on Pt(111) is found to be significantly lower (circa 0.13 eV at 0 $V_{SHE}$ using the ice bilayer model and the PBE functional). For this water structure, we do observe a larger difference between RPBE and PBE, with activation energies of respectively 0.69 and 0.50 eV according to our calculations. Further investigation will be needed to explain the remaining difference, e.g. whether or not it is due to the simplified description of the countercharge distribution. Describing this distribution using a jellium slab close to the electrode (with a width equal to the Debye length) would be expected to be appropriate only in the limit of very high ionic strengths.

## $H_2$ evolution on Pt(110)-(1×2)

We now turn to the missing-row reconstructed Pt(110) surface, with a hydrogen coverage of 1 ML where all ridge and (micro-)facet sites are occupied (see Panel (b) in Figure 4). Although there is a weak thermodynamic preference for the adsorption of additional hydrogen atoms in the trough sites at $U_{SHE} = 0$ V (with differential binding energies of circa 0.1 eV),[6,63,64] it will be argued below that trough-adsorbed hydrogen atoms, if present, would not contribute significantly to the hydrogen evolution rate at 0 V.

Panel (a) in Figure 4 shows the calculated barrier heights for several relevant Volmer and Tafel steps at and below 1 ML coverage of hydrogen. Various attempts at locating saddle points for the Heyrovský reactions converged to Volmer-like saddle points, suggesting that these reactions are inoperable on this surface. On both types of sites, the Tafel reaction proceeds via an intermediate corresponding to a

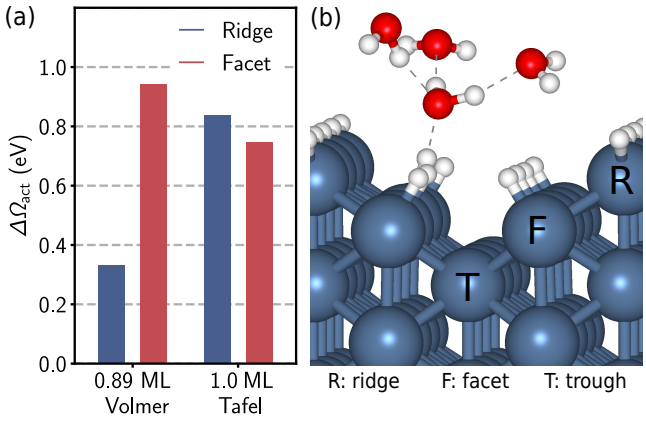


Figure 4: Panel (a): barrier heights calculated at 0 $V_{SHE}$ for the Volmer and Tafel processes on the Pt(110)-(1×2) surface. Panel (b): structural model of the transition state at 0 $V_{SHE}$ for the Volmer reaction on a (micro-)facet.

Kubas complex,[65] consisting of a stretched hydrogen molecule on top of a platinum atom (see Figure 5). Desorption of $H_2$ via the Tafel reaction is faster on the facet (0.75 eV) compared to the ridge (0.84 eV). This is in line with the higher binding energy of the ridge-bound adatoms. These results are comparable to calculations in the literature using the same functional and hydrogen coverage, but without solvent and at the potential of zero charge.[6,64]

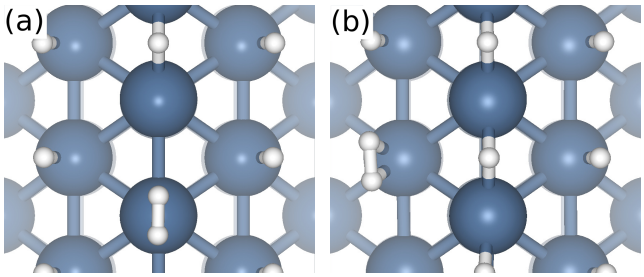


Figure 5: Structural models of the Kubas complex as an intermediate of the Tafel reaction at 0 $V_{SHE}$ on ridges (a) and microfacets (b) of the Pt(110)-(1×2) surface.

Similarly, at an initial hydrogen coverage of 0.89 ML, we find a higher barrier for the Volmer step on the facets (0.94 eV) compared to the ridge (0.33 eV). This change exceeds the difference in hydrogen binding energy between the two site types (calculated to be only 0.23 eV). Hence, even though hydrogen desorption will take place on the facets, replenishment of the

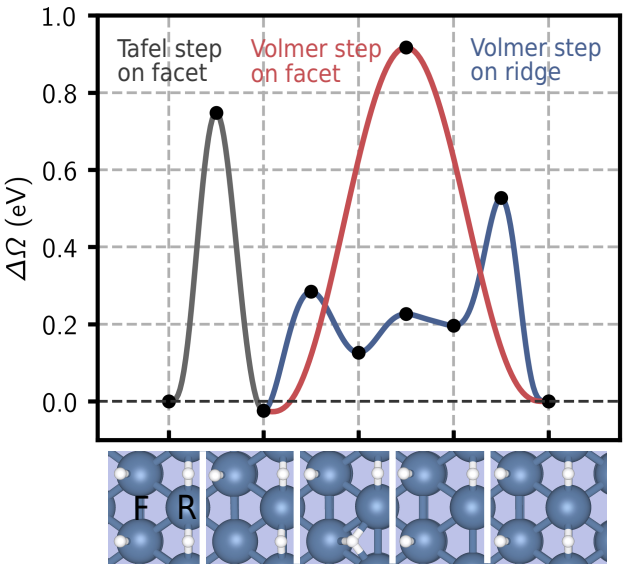


Figure 6: Calculated energy diagram for HER on Pt(110)-(1×2) at at 0 $V_{SHE}$ for a steady-state hydrogen coverage of 1 ML. The reaction energies have been evaluated using the CHE formalism.

coverage happens most rapidly via diffusion of H atoms from the ridge to the vacant facet sites followed by Volmer discharge on the now-vacant ridge site. This process is illustrated in the energy diagram in Figure 6. As the diffusion barrier is low (0.3 eV), the Volmer step will dictate the apparent activation energy, which then amounts to 0.56 eV. This entails that hydrogen deposition is fast relative to the Tafel reaction, making the latter the RDS. This is in qualitative agreement with the measurements on a Pt(110) single-crystal by Marković and coworkers,[35] where the same RDS is found. The reported activation energy (0.1 eV) is much lower than suggested by our calculations (0.75 eV), but is likely to be an underestimate due to a low concentration of highly active defect sites, as has been argued in the case of Pt(111).[62] The relative activities of the (111) and (110)-(1×2) surfaces are, however, in good agreement, as the apparent activation energy is circa 0.1 eV lower on Pt(110)-(1×2) than on Pt(111) according to the experiments as well as the present calculations.

We now return to the question whether hydrogen coverages beyond 1 ML (with occupations of trough sites) could be relevant at

$U = 0$ $V_{SHE}$. Firstly, the relatively high barrier obtained for the Volmer reaction on the facet suggests that the corresponding barrier on the trough will be even higher, requiring a similar diffusion-assisted mechanism as described above. However, moving a ridge-bound H atom to a trough position requires more energy (0.46 eV) than to a facet site. Achieving a significant occupation of the trough sites is, therefore, kinetically difficult. Additionally, even if a partial occupation of the trough sites would be reached, the Tafel reaction on the facets would remain the main desorption pathway for hydrogen. Previous studies have namely found that, despite the lower binding energy, the barrier for hydrogen desorption from trough sites is larger compared to the facet sites when the hydrogen coverage is at or slightly beyond 1 ML.[63,64] It is therefore sufficient to only consider ridge- and facet-bound hydrogen atoms for HER on Pt(110)-(1×2) at 0 $V_{SHE}$.

# Conclusions

We have evaluated the performance of a recently developed constant-potential implicit solvation approach to electrochemical barriers for one of the classical processes in catalysis, the hydrogen evolution reaction on platinum. The relevant Volmer, Tafel, and Heyrovský kinetics on Pt(111) and Pt(110) at 0 V versus SHE compare well with the previously developed 'extrapolation' approach and with available experimental data. Importantly, the inclusion of an implicit solvent only moderately increases the computational cost, whereas calculating barrier heights with the extrapolation approach is more expensive by at least one order of magnitude. Care should be taken, however, in dealing with spurious electrostatic interactions between periodically repeated slabs when using the VASPsol code.

Although further testing for other types of reactions and materials is warranted, we have so far found the accuracy to be satisfactory and expect implicit solvation approaches to receive increasing attention in future research. The application and continued development of cost-effective methods is most welcome, as the previous lack of such approaches has frequently led to kinetic aspects being disregarded in first-principles electrocatalysis research.

**Acknowledgement** The authors thank Vitae Industries for providing computational resources, and Javed Hussain for valuable discussions. This material is based upon work supported by the National Science Foundation under Grant No. CHE-1665372.

# Supporting Information Available

Coordinate files pertaining to the hydrogen evolution reactions on Pt(111) and Pt(110).

# References

(1) Nørskov, J. K.; Rossmeisl, J.; Logadottir, A.; Lindqvist, L.; Kitchin, J. R.; Bligaard, T.; Jónsson, H. Origin of the Overpotential for Oxygen Reduction at a Fuel-Cell Cathode. *J. Phys. Chem. B* **2004**, *108*, 17886–17892.

(2) Nørskov, J. K.; Bligaard, T.; Logadottir, A.; Kitchin, J. R.; Chen, J. G.; Pandelov, S.; Stimming, U. Trends in the Exchange Current for Hydrogen Evolution. *J. Electrochem. Soc.* **2005**, *152*, J23–J26.

(3) Skúlason, E.; Jónsson, H. Atomic Scale Simulations of Heterogeneous Electrocatalysis: Recent Advances. *Adv. Phys. X* **2017**, *2*, 481–495.

(4) Exner, K. S.; Over, H. Kinetics of Electrocatalytic Reactions from First-Principles: A Critical Comparison with the Ab Initio Thermodynamics Approach. *Acc. Chem. Res.* **2017**, *50*, 1240–1247.

(5) Rossmeisl, J.; Skúlason, E.; Björketun, M. E.; Tripkovic, V.; Nørskov, J. K. Modeling the Electrified Solid-Liquid Interface. *J. Chem. Phys. Lett.* **2008**, *466*, 68–71.

(6) Skúlason, E.; Tripkovic, V.; Björketun, M. E.; Gudmundsdóttir, S.; Karlberg, G.; Rossmeisl, J.; Bligaard, T.; Jónsson, H.; Nørskov, J. K. Modeling the Electrochemical Hydrogen Oxidation and Evolution Reactions on the Basis of Density Functional Theory Calculations. *J. Phys. Chem. C* **2010**, *114*, 18182–18197.

(7) Skúlason, E.; S. Karlberg, G.; Rossmeisl, J.; Bligaard, T.; Greeley, J.; Jónsson, H.; K. Nørskov, J. Density Functional Theory Calculations for the Hydrogen Evolution Reaction in an Electrochemical Double Layer on the Pt(111) Electrode. *Phys. Chem. Chem. Phys.* **2007**, *9*, 3241–3250.

(8) Hussain, J.; Jónsson, H.; Skúlason, E. Faraday Efficiency and Mechanism of Electrochemical Surface Reactions: $CO_2$ Reduction and $H_2$ Formation on Pt(111). *Faraday Discuss.* **2016**, *195*, 619–636.

(9) Hussain, J.; Jónsson, H.; Skúlason, E. Calculations of Product Selectivity in Electrochemical $CO_2$ Reduction. *ACS Catal.* **2018**, 5240–5249.

(10) Chan, K.; Nørskov, J. K. Electrochemical Barriers Made Simple. *J. Phys. Chem. Lett.* **2015**, *6*, 2663–2668.

(11) Chan, K.; Nørskov, J. K. Potential Dependence of Electrochemical Barriers from ab Initio Calculations. *J. Phys. Chem. Lett.* **2016**, *7*, 1686–1690.

(12) Filhol, J.-S.; Neurock, M. Elucidation of the Electrochemical Activation of Water over Pd by First Principles. *Angew. Chem. Int. Ed.* **2006**, *45*, 402–406.

(13) Taylor, C. D.; Wasileski, S. A.; Filhol, J.-S.; Neurock, M. First Principles Reaction Modeling of the Electrochemical Interface: Consideration and Calculation of a Tunable Surface Potential from Atomic and Electronic Structure. *Phys. Rev. B* **2006**, *73*, 165402.

(14) Makov, G.; Payne, M. C. Periodic Boundary Conditions in Ab Initio Calculations. *Phys. Rev. B* **1995**, *51*, 4014–4022.

(15) Komsa, H.-P.; Rantala, T. T.; Pasquarello, A. Finite-Size Supercell Correction Schemes for Charged Defect Calculations. *Phys. Rev. B* **2012**, *86*, 045112.

(16) Otani, M.; Hamada, I.; Sugino, O.; Morikawa, Y.; Okamoto, Y.; Ikeshoji, T. Structure of the Water/Platinum Interface – a First Principles Simulation Under Bias Potential. *Phys. Chem. Chem. Phys.* **2008**, *10*, 3609–3612.

(17) Surendralal, S.; Todorova, M.; Finnis, M. W.; Neugebauer, J. First-Principles Approach to Model Electrochemical Reactions: Understanding the Fundamental Mechanisms behind Mg Corrosion. *Phys. Rev. Lett.* **2018**, *120*, 246801.

(18) Akhade, S. A.; Bernstein, N. J.; Esopi, M. R.; Regula, M. J.; Janik, M. J. A Simple Method to Approximate Electrode Potential-Dependent Activation Energies Using Density Functional Theory. *Catal. Today* **2017**, *288*, 63–73.

(19) Akhade, S. A.; Nidzyn, R. M.; Rostamikia, G.; Janik, M. J. Using Brønsted-Evans-Polanyi Relations to Predict Electrode Potential-Dependent Activation Energies. *Catal. Today* **2018**, *312*, 82–91.

(20) Sundararaman, R.; Goddard, W. A.; Arias, T. A. Grand Canonical Electronic Density-Functional Theory: Algorithms and Applications to Electrochemistry. *J. Chem. Phys.* **2017**, *146*, 114104.

(21) Sundararaman, R.; Letchworth-Weaver, K.; Schwarz, K. A.; Gunceler, D.; Ozhabes, Y.; Arias, T. A. JDFTx: Software for Joint Density-Functional Theory. *SoftwareX* **2017**, *6*, 278–284.

(22) Mathew, K.; Sundararaman, R.; Letchworth-Weaver, K.; Arias, T. A.;

Hennig, R. G. Implicit Solvation Model for Density-Functional Study of Nanocrystal Surfaces and Reaction Pathways. *J. Chem. Phys.* **2014**, *140*, 084106.

(23) Mathew, K.; Hennig, R. G. Implicit Self-Consistent Description of Electrolyte in Plane-Wave Density-Functional Theory. *arXiv:1601.03346 [cond-mat]* **2016**, arXiv: 1601.03346.

(24) Goodpaster, J. D.; Bell, A. T.; Head-Gordon, M. Identification of Possible Pathways for C-C Bond Formation during Electrochemical Reduction of $CO_2$: New Theoretical Insights from an Improved Electrochemical Model. *J. Phys. Chem. Lett.* **2016**, *7*, 1471–1477.

(25) Singh, M. R.; Goodpaster, J. D.; Weber, A. Z.; Head-Gordon, M.; Bell, A. T. Mechanistic Insights into Electrochemical Reduction of $CO_2$ Over Ag Using Density Functional Theory and Transport Models. *PNAS* **2017**, *114*, E8812–E8821.

(26) Garza, A. J.; Bell, A. T.; Head-Gordon, M. Is Subsurface Oxygen Necessary for the Electrochemical Reduction of $CO_2$ on Copper? *J. Phys. Chem. Lett.* **2018**, *9*, 601–606.

(27) Garza, A. J.; Bell, A. T.; Head-Gordon, M. Mechanism of $CO_2$ Reduction at Copper Surfaces: Pathways to $C_2$ Products. *ACS Catal.* **2018**, *8*, 1490–1499.

(28) Schwarz, K. A.; Sundararaman, R.; Moffat, T. P.; Allison, T. C. Formic Acid Oxidation on Platinum: A Simple Mechanistic Study. *Phys. Chem. Chem. Phys.* **2015**, *17*, 20805–20813.

(29) Wang, H.-F.; Liu, Z.-P. Formic Acid Oxidation at $Pt/H_2O$ Interface from Periodic DFT Calculations Integrated with a Continuum Solvation Model. *J. Phys. Chem. C* **2009**, *113*, 17502–17508.

(30) Fang, Y.; Liu, Z. Electrochemical Reactions at the Electrode/Solution Interface: Theory and Applications to Water Electrolysis and Oxygen Reduction. *Sci. China Chem.* **2010**, *53*, 543–552.

(31) Fang, Y.-H.; Wei, G.-F.; Liu, Z.-P. Catalytic Role of Minority Species and Minority Sites for Electrochemical Hydrogen Evolution on Metals: Surface Charging, Coverage, and Tafel Kinetics. *J. Phys. Chem. C* **2013**, *117*, 7669–7680.

(32) Fang, Y.-H.; Wei, G.-F.; Liu, Z.-P. Theoretical Modeling of Electrode/Electrolyte Interface from First-Principles Periodic Continuum Solvation Method. *Catal. Today* **2013**, *202*, 98–104.

(33) Fang, Y.-H.; Liu, Z.-P. Tafel Kinetics of Electrocatalytic Reactions: From Experiment to First-Principles. *ACS Catal.* **2014**, *4*, 4364–4376.

(34) Kastlunger, G.; Lindgren, P.; Peterson, A. A. Controlled-Potential Simulation of Elementary Electrochemical Reactions: Proton Discharge on Metal Surfaces. *J. Phys. Chem. C* **2018**,

(35) Marković, N. M.; Grgur, B. N.; Ross, P. N. Temperature-Dependent Hydrogen Electrochemistry on Platinum Low-Index Single-Crystal Surfaces in Acid Solutions. *J. Phys. Chem. B* **1997**, *101*, 5405–5413.

(36) Kresse, G.; Hafner, J. Ab Initio Molecular-Dynamics Simulation of the Liquid-Metal-Amorphous-Semiconductor Transition in Germanium. *Phys. Rev. B* **1994**, *49*, 14251–14269.

(37) Kresse, G.; Furthmüller, J. Efficiency of Ab-Initio Total Energy Calculations for Metals and Semiconductors Using a Plane-Wave Basis Set. *Comp. Mater. Sci.* **1996**, *6*, 15–50.

(38) Kresse, G.; Furthmüller, J. Efficient Iterative Schemes for Ab Initio Total-Energy Calculations Using a Plane-Wave Basis Set. *Phys. Rev. B* **1996**, *54*, 11169–11186.

(39) Kresse, G.; Joubert, D. From Ultrasoft Pseudopotentials to the Projector

Augmented-Wave Method. *Phys. Rev. B* **1999**, *59*, 1758–1775.

(40) Hohenberg, P.; Kohn, W. Inhomogeneous Electron Gas. *Phys. Rev.* **1964**, *136*, B864–B871.

(41) Kohn, W.; Sham, L. J. Self-Consistent Equations Including Exchange and Correlation Effects. *Phys. Rev.* **1965**, *140*, A1133–A1138.

(42) Garrity, K. F.; Bennett, J. W.; Rabe, K. M.; Vanderbilt, D. Pseudopotentials for High-Throughput DFT Calculations. *Comp. Mater. Sci.* **2014**, *81*, 446–452.

(43) Hammer, B.; Hansen, L. B.; Nørskov, J. K. Improved Adsorption Energetics Within Density-Functional Theory Using Revised Perdew-Burke-Ernzerhof Functionals. *Phys. Rev. B* **1999**, *59*, 7413–7421.

(44) Perdew, J. P.; Burke, K.; Ernzerhof, M. Generalized Gradient Approximation Made Simple. *Phys. Rev. Lett.* **1996**, *77*, 3865–3868.

(45) Marques, M. A. L.; Oliveira, M. J. T.; Burnus, T. Libxc: A Library of Exchange and Correlation Functionals for Density Functional Theory. *Computer Physics Communications* **2012**, *183*, 2272–2281.

(46) Monkhorst, H. J.; Pack, J. D. Special Points for Brillouin-Zone Integrations. *Phys. Rev. B* **1976**, *13*, 5188–5192.

(47) Pack, J. D.; Monkhorst, H. J. 'Special Points for Brillouin-Zone Integrations' – a Reply. *Phys. Rev. B* **1977**, *16*, 1748–1749.

(48) Henkelman, G.; Jónsson, H. A Dimer Method for Finding Saddle Points on High Dimensional Potential Surfaces Using Only First Derivatives. *J. Chem. Phys.* **1999**, *111*, 7010–7022.

(49) Olsen, R. A.; Kroes, G. J.; Henkelman, G.; Arnaldsson, A.; Jónsson, H. Comparison of Methods for Finding Saddle Points Without Knowledge of the Final States. *J. Chem. Phys.* **2004**, *121*, 9776–9792.

(50) Gunceler, D.; Letchworth-Weaver, K.; Sundararaman, R.; Schwarz, K. A.; Arias, T. A. The Importance of Nonlinear Fluid Response in Joint Density-Functional Theory Studies of Battery Systems. *Modelling Simul. Mater. Sci. Eng.* **2013**, *21*, 074005.

(51) Andreussi, O.; Dabo, I.; Marzari, N. Revised Self-Consistent Continuum Solvation in Electronic-Structure Calculations. *J. Chem. Phys.* **2012**, *136*, 064102.

(52) Murrell, J.; Jenkins, A. *Properties of Liquids and Solutions*, 2nd ed.; Wiley & Sons: Chichester, England, 1994.

(53) Trasatti, S. The Absolute Electrode Potential: An Explanatory Note (recommendations 1986). *Pure Appl. Chem.* **1986**, *58*, 955–966.

(54) Melander, M.; Kuisma, M.; Christensen, T.; Honkala, K. *Grand-Canonical Approach to Density Functional Theory of Electrocatalytic Systems: Thermodynamics of Solid-Liquid Interfaces at Constant Ion and Electrode Potentials*; ChemRxiv, 2018.

(55) Sundararaman, R.; Arias, T. A. Regularization of the Coulomb singularity in exact exchange by Wigner-Seitz truncated interactions: Towards chemical accuracy in nontrivial systems. *Phys. Rev. B* **2013**, *87*, 165122.

(56) Steinmann, S. N.; Ferreira De Morais, R.; Götz, A. W.; Fleurat-Lessard, P.; Iannuzzi, M.; Sautet, P.; Michel, C. Force Field for Water over Pt(111): Development, Assessment, and Comparison. *J. Chem. Theory Comput.* **2018**, *14*, 3238–3251.

(57) Le, J.; Iannuzzi, M.; Cuesta, A.; Cheng, J. Determining Potentials of Zero Charge

of Metal Electrodes versus the Standard Hydrogen Electrode from Density-Functional-Theory-Based Molecular Dynamics. *Phys. Rev. Lett.* **2017**, *119*, 016801.

(58) Meng, S.; Xu, L. F.; Wang, E. G.; Gao, S. Vibrational Recognition of Hydrogen-Bonded Water Networks on a Metal Surface. *Phys. Rev. Lett.* **2002**, *89*, 176104.

(59) Ogasawara, H.; Brena, B.; Nordlund, D.; Nyberg, M.; Pelmenschikov, A.; Pettersson, L. G. M.; Nilsson, A. Structure and Bonding of Water on Pt(111). *Phys. Rev. Lett.* **2002**, *89*, 276102.

(60) Schnur, S.; Groß, A. Properties of Metal-Water Interfaces Studied from First Principles. *New J. Phys.* **2009**, *11*, 125003.

(61) Groß, A.; Gossenberger, F.; Lin, X.; Naderian, M.; Sakong, S.; Roman, T. Water Structures at Metal Electrodes Studied by Ab Initio Molecular Dynamics Simulations. *J. Electrochem. Soc.* **2014**, *161*, E3015–E3020.

(62) He, Z.-D.; Wei, J.; Chen, Y.-X.; Santos, E.; Schmickler, W. Hydrogen Evolution at Pt(111) - Activation Energy, Frequency Factor and Hydrogen Repulsion. *Electrochim. Acta* **2017**, *255*, 391–395.

(63) Gudmundsdóttir, S.; Skúlason, E.; Jónsson, H. Reentrant Mechanism for Associative Desorption: $H_2$/Pt(110)-(1×2). *Phys. Rev. Lett.* **2012**, *108*, 156101.

(64) Gudmundsdóttir, S.; Skúlason, E.; Weststrate, K.-J.; Juurlink, L.; Jónsson, H. Hydrogen Adsorption and Desorption at the Pt(110)-(1×2) Surface: Experimental and Theoretical Study. *Phys. Chem. Chem. Phys.* **2013**, *15*, 6323–6332.

(65) Kubas, G. J. Molecular Hydrogen Complexes: Coordination of a $\sigma$ Bond to Transition Metals. *Acc. Chem. Res.* **1988**, *21*, 120–128.

# TOC Graphic

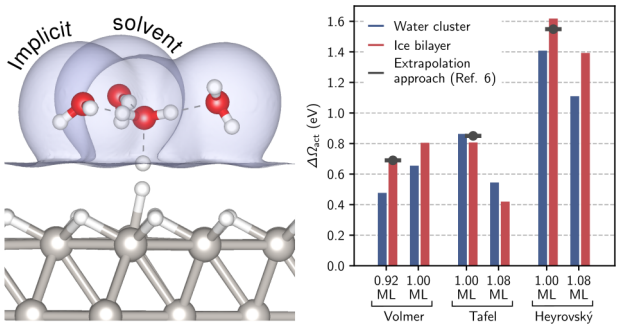
Implicit solvent
Water cluster
Ice bilayer
Extrapolation approach (Ref. 6)
$\Delta\Omega_{act}$ (eV)
0.0
0.2
0.4
0.6
0.8
1.0
1.2
1.4
1.6
0.92 ML
1.00 ML
1.00 ML
1.08 ML
1.00 ML
1.08 ML
Volmer
Tafel
Heyrovský